communications biology

Article

https://doi.org/10.1038/s42003-024-06952-6

Rapid predator-prey balance shift follows critical-population-density transmission between cod (*Gadus morhua*) and capelin (*Mallotus villosus*)

Shourav Pednekar[1], Ankita Jain[1], Olav Rune Godø[2,3] & Nicholas C. Makris[1]

Sensing limitations have impeded knowledge about how individual predator-prey interactions build to organized multi-species group behaviour across an ecosystem. Population densities of overlapping interacting oceanic fish predator and prey species, however, can be instantaneously distinguished and quantified from roughly the elemental individual to spatial scales spanning thousands of square kilometres by wide-area multispectral underwater-acoustic sensing, as shown here. This enables fundamental mechanisms behind large-scale ordered predator-prey interactions to be investigated. Critical population densities that transition random individual behaviour to ordered group behaviour are found to rapidly propagate to form vast adversarial prey and predator shoals of capelin and surrounding cod in the Barents Sea Arctic ecosystem for these keystone species. This leads to a sudden major shift in predator-prey balance. Only a small change in local behaviour triggers the shift due to an unstable equilibrium. Such unstable equilibria and associated balance shifts at predation hotspots are often overlooked as blind spots in present ocean ecosystem monitoring and assessment due to use of highly undersampled spatio-temporal sampling methods.

Seasonal spawning migration of capelin (Mallotus villosus) from offshore waters of the Barents Sea to the Norwegian coast precedes heavy predation by Atlantic cod (Gadus morhua), their primary predator, on or close to capelin spawning grounds near Finnmark[1,2]. A mixture of large immature cod and maturing cod migrate to the coast to feed on capelin before the mature cod continue their migration to the more southerly cod spawning grounds at Lofoten. This setting created by the spatial overlap between capelin and cod populations inhabiting the Northeast Atlantic in February–March every year is an ideal hotspot for studying large-scale predator-prey interactions. Similar hotspots have been identified in other Arctic ecosystems[3,4], but such hotspots are largely unexplored features in marine ecosystems with potential importance for management[5].

We employ Ocean Acoustic Waveguide Remote Sensing (OAWRS)[6–11], with a significant multi-spectral adaptation, to quantify cod-capelin interactions from the near individual to scales spanning many tens of kilometres. The multi-spectral adaptation employs sensing frequencies at or near fish swimbladder resonance where the large differences across fish species are discernible and long-range ocean acoustic waveguide propagation is possible. This subsequently enables the population density of overlapping cod and capelin fields to be instantaneously distinguished with high resolution over thousands of square kilometres at all pixels in an Eulerian frame and then monitored with minute-to-minute updates. In contrast, conventional methods survey each species separately following a Lagrangian track along widely spaced line transects, traversed by a slowly moving research vessel with areal sampling rate roughly one million times lower than the method used here[6]. The independent acoustic line transect surveys for predator and prey in conventional approaches are then analysed to infer highly averaged parameters of the potential interactions without direct measurement of the interactions[12–14].

The much higher sampling rate and intrinsically Eulerian frame of the sensing method used here enables dynamic interactions between predator and prey to be directly sensed over wide areas with high resolution in space and time. It also enables direct wide-area measurement of the propagation of critical population density, which is a fundamental threshold in animal group behaviour[6,11,15–17]. Critical density occurs when spheres of perception overlap and lead to a chain reaction where individuals take on the mean behaviour of similar entities they sense. Random individual motion then transitions to ordered group behaviour and population density rapidly

[1]Department of Mechanical Engineering, Massachusetts Institute of Technology, Cambridge, USA. [2]Institute of Marine Research, Post Office Box 1870 Bergen, Norway. [3]Husgod Holding AS, Nesttun, Norway. e-mail: makris@mit.edu

increases[15]. The critical density transition from disorder to order has been shown to occur within species[6,16,17] and to lead to the formation of vast spawning shoals[6,11], but has not been previously found to simultaneously propagate across species over wide areas, which is the focus of this study.

Critical population density has also not been previously linked to unstable equilibria that yield shifts in predator-prey balance as found here. Familiar natural examples of unstable equilibria, where small local changes lead to large and sudden transfers of energy and state, include avalanches, earthquakes, volcanic eruptions and forest fires, all of which are governed by physical laws[18–20]. In large natural ecosystems that occupy most of the earth's surface and ocean volume, however, the ordered behavioural mechanisms governing unstable equilibria between interacting predators and prey populations typically remain elusive due to sensing limitations[21–25]. It is through these unstable equilibria, however, that ocean ecosystems are likely extremely vulnerable to the increasing stresses of overexploitation, climate change and ocean industrialization. Reduction of population densities from these stresses will eventually curtail the critical density processes described here. The extended time needed to rebuild depleted oceanic stocks is likely also related to the time it takes to re-establish population density-dependent behavioural processes of the kind observed here.

It is the goal of this paper to quantify population density-dependent mechanisms governing behavioural processes within and across species. With this information, we aim to describe the dynamics of predator-prey interaction at predation hotspots, and to specifically estimate cod predation on capelin at and around capelin spawning grounds.

Results

Ordered group behaviour rapidly propagates between cod predators and capelin prey on attaining respective critical population densities

During the capelin spawning season, diffuse low density capelin (Fig. 1a(i)) and sporadic clusters of large cod (Fig. 1b(i)) were found along the capelin's migration route from the ice-edge to their traditional spawning ground[2] along Finnmark, Norway, on February 27, 2014 within tens of kilometres of the coast (Fig. 2a). Capelin population densities remained stable until a critical population density was attained, roughly 10 minutes after the onset of dawn twilight (Fig. 3a). Capelin population density in specific locations then rapidly increased (Fig. 3a) and propagated horizontally as density waves, faster than the capelin swimming speed (Fig. 4a), to form dense lineated shoals together stretching for over 10 km. Outside the shoals, capelin population density remained low and stable indicating no change from disordered to ordered group behaviour (Fig. 1a(i–iii), Supplementary Data 1). The shoals proceeded to coherently migrate normal to their axes at roughly 0.15 m/s in accord with expected capelin swimming speeds. Such behaviour has not been previously documented nor quantified in capelin, but has been observed in other fish species[6]. Coherent migration in shoals has been demonstrated to be energy saving[26] and provides a significant group behavioural advantage. With this, capelin likely employ established correlated group hydrodynamic flow mechanisms to swim efficiently enough to traverse the great distances necessary to accomplish their essential migration from ice-edge feeding to coastal spawning grounds. At the onset of shoal formation at twilight's dawn, capelin began to slowly descend from their shallow night layer within 50-m of the sea surface (Fig. 2c). The shoal increased in density as it descended towards the seafloor (Figs. 1a, 3a), possibly in search of appropriate spawning locations or necessary pre-spawning conditions, or possibly to avoid being seen more readily by predators in the emerging near surface light.

The instantaneously imaged dense capelin shoals are estimated to contain roughly 23 million individuals and weigh 414 tons (Fig. 1a(ii)), roughly 0.1% of the Barents Sea capelin spawning stock (~ 500000 tons[27]) with roughly 68.5 million in the entire region of Fig. 1a(ii), before entering the predatory cod layer. The capelin shoals are defined by regions where population density is above the critical density of 1.4 capelin/m^2, which is roughly three times higher than the mean capelin density in the diffuse regions outside the shoal boundaries. The highest concentrations ranged from 20 to 30 capelin/m^2 in the interior of the shoals at multiple population centres, consistent with expected shoaling densities[28]. The capelin critical density scales roughly in inverse proportion to fish-length-squared when compared with findings from other species, as expected[6,11,29,30]. There is an offset percentage error in our capelin population estimates of ±25% due to statistical variation in capelin length (Methods), which is not large enough to affect the analysis and conclusions.

At dawn cod attained critical population density transitioning from unorganized individual to ordered group behaviour with rapidly increasing population density (Fig. 3b). The inception locations were coincident with the forming capelin shoal. From these inception locations both capelin and cod shoals rapidly propagated outward over large areas, a cross-species phenomenon not previously observed. This began at a time indistinguishable from that of the capelin attaining critical population density (Fig. 3, Supplementary Data 2). So, it is unclear if the cod or capelin transitioned first

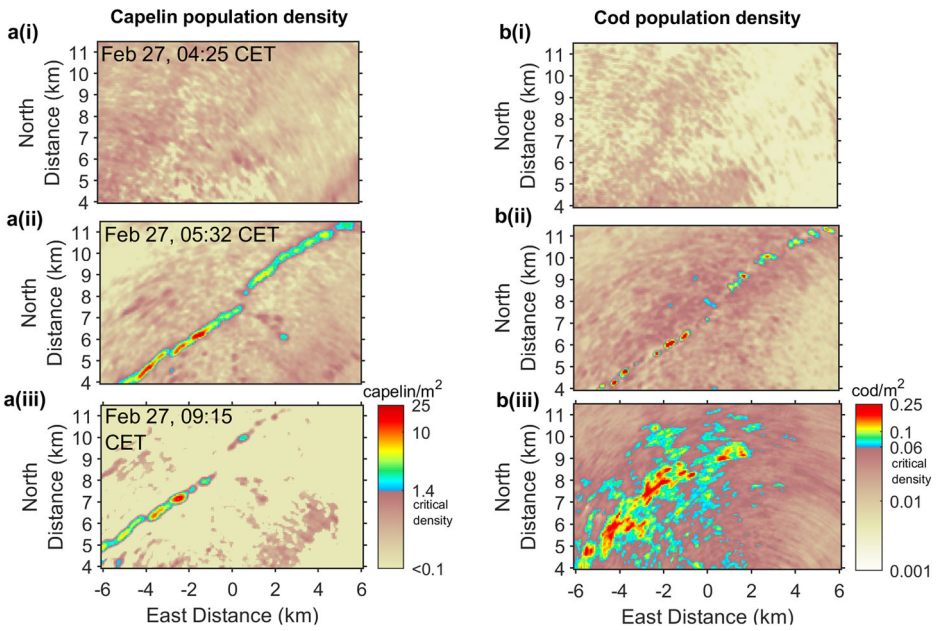

Fig. 1 | Instantaneous wide area population density images of overlapping species showing transition from random individual behaviour to ordered adversarial group behaviour in rapid formation and propagation of capelin prey and engulfing cod predator shoals. a Capelin and **b** cod population density measured with multi-spectral ocean-acoustic-waveguide remote sensing[5,6] showing diffuse randomly moving predawn capelin **a(i)** and cod **b(i)** near capelin spawning grounds, Finnmark Norway. **a(ii)** Coherently migrating lineated capelin shoals abruptly form at dawn that **b(ii)** simultaneously forming cod shoals begin to engulf. **a(iii)** Surviving capelin when **b(iii)** measured vast engulfing cod shoal is fully formed.

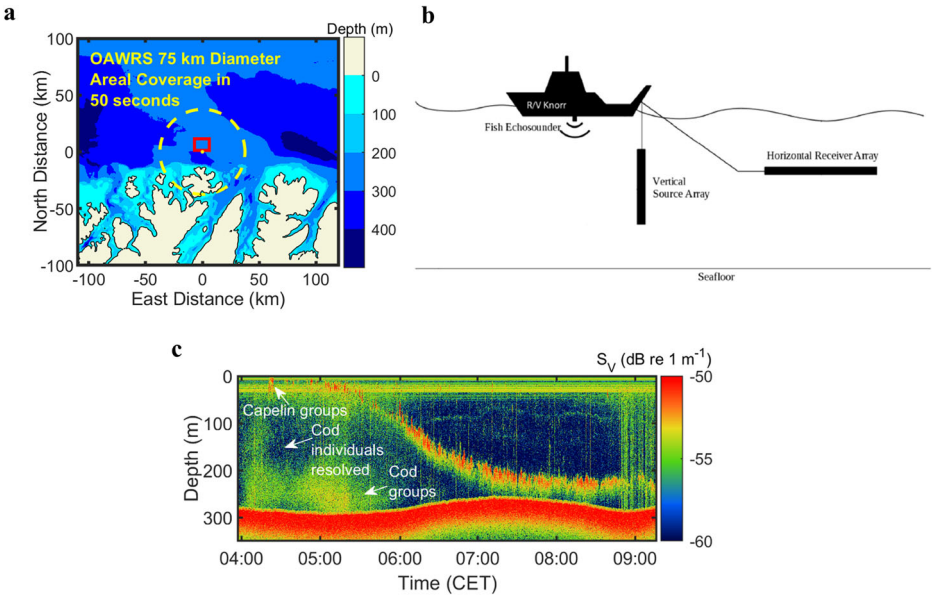

Fig. 2 | Ocean Acoustic Waveguide Remote Sensing (OAWRS) instantaneous areal coverage in a region with spatially overlapping capelin and cod populations. a Bathymetry near Nordkapp, Finnmark. Yellow circle marks areal coverage in 50 s of ocean-acoustic-waveguide remote sensing system on RV Knorr, whose location at 5:35 CET corresponds to coordinate origin (71.2944° North, 25.7193° East) in Fig. 1a, b. Red box indicates boundaries of Fig. 1a, b zoom on adversarial shoals. **b** OAWRS physical setup on RV Knorr towing the source and receiver arrays. **c** Echogram shows predawn capelin are near sea surface with individual widely spaced cod beneath them. Shortly after dawn twilight (04:39 CET) capelin slowly descend towards seafloor through depths inhabited by cod who are visual predators. Capelin arrive at seafloor near sunrise (07:00 CET). Conventional echogram from RV Knorr depth-sounder showing multispecies volume backscattering strength, S_V[73].

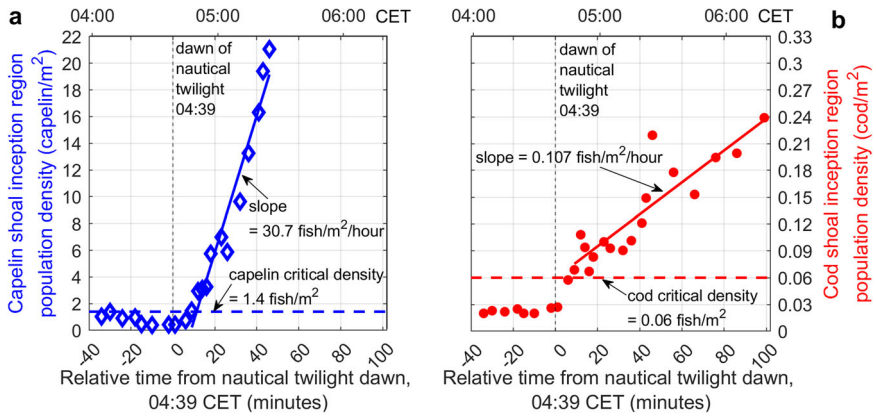

Fig. 3 | Quantifying critical population density transition from random individual to organized group behaviour as it rapidly propagates within and across prey and predator fields. a,b Population densities versus time from multi-spectral ocean acoustic waveguide remote sensing data. Population density is temporally stable for both **a** capelin and **b** cod before dawn twilight (04:39 CET). Just after twilight dawn both **a** capelin and **b** cod population densities rapidly increase after respective critical thresholds are attained at inception region **a** centred at (−1.57, 6.10) for capelin and **b** centred at (−1.83, 5.88) for cod in Fig. 1 coordinates, each spanning 200 × 200 m^2. Critical population density then rapidly spreads from inception regions to form the vast dense shoals of Fig. 1, a(ii,iii), b(ii,iii).

or if both transitioned simultaneously at these initial locations. While change in light level appears to have been the trigger, critical population density was transmitted across species and led to the simultaneous or nearly simultaneous inception and subsequent propagation of rapidly forming capelin and engulfing cod shoals (Fig. 1bii–iii). Cod shoal formation, like that of the capelin shoals, propagated as density waves travelling faster than the constituent fish can swim (Fig. 4b).

Catch samples from the survey region confirmed the predatory nature of the engulfing cod in that all cod caught had numerous capelin within their digestive system. Cod, as visual predators, are expected to feed in the periphery of shoals, as is consistent with our echogram data (Fig. 2c). Hunting by shoals of predators is considered to be more efficient than hunting by individuals, since a predatory shoal is able to break a prey shoal, releasing individuals that become easy targets for predation[31]. These individuals that are not able to find the safest position in shoal likely belong to the weaker component of the shoal, in accordance with the selfish herd theory[32]. Critical density for the cod shoal was found to be 0.06 cod/m^2, again roughly scaling in inverse proportion to fish length squared when compared to that found for capelin here and Atlantic herring and mature cod previously[6,11]. The size of the cod shoal, above cod critical density, engulfing the capelin shoal continued to steadily increase in size as a propagating wave through previously diffuse cod at a speed much faster than cod swim even after the capelin shoal reached the seafloor (Fig. 4b, Supplementary Data 3). Besides the benefit of increased visibility as dawn progressed, cod convergence may have been facilitated by intentional or accidental acoustic signalling, since cod are known to produce low frequency sound[33]. We studied the potential impact of other swimbladder-bearing fish in the analysis of our acoustic data. Based on information of density distributions, behavioural characteristics and swimbladder sizes of other species including haddock, herring, blue whiting and Sebastes, as observed by the simultaneous winter survey[34], and OAWRS scattering analysis with mixed species[9], the error in our cod population density estimates from potential contamination from species other than cod is found to be less 10% (Methods).

Local behavioural changes lead to vast predator-prey balance shift

An abrupt increase in areal consumption rate of capelin by cod occurs in the capelin shoal (Fig. 5a–c). A similarly abrupt change in predator-to-prey balance occurs in the capelin shoal (Fig. 5d). As the population density of cod engulfing the capelin shoals rapidly increases, the estimated number of capelin consumed rapidly increases (Fig. 5, Supplementary Data 4). Total population of cod above critical population density of 0.06 fish/m^2 rises to roughly 2.5 million in the imaged area.

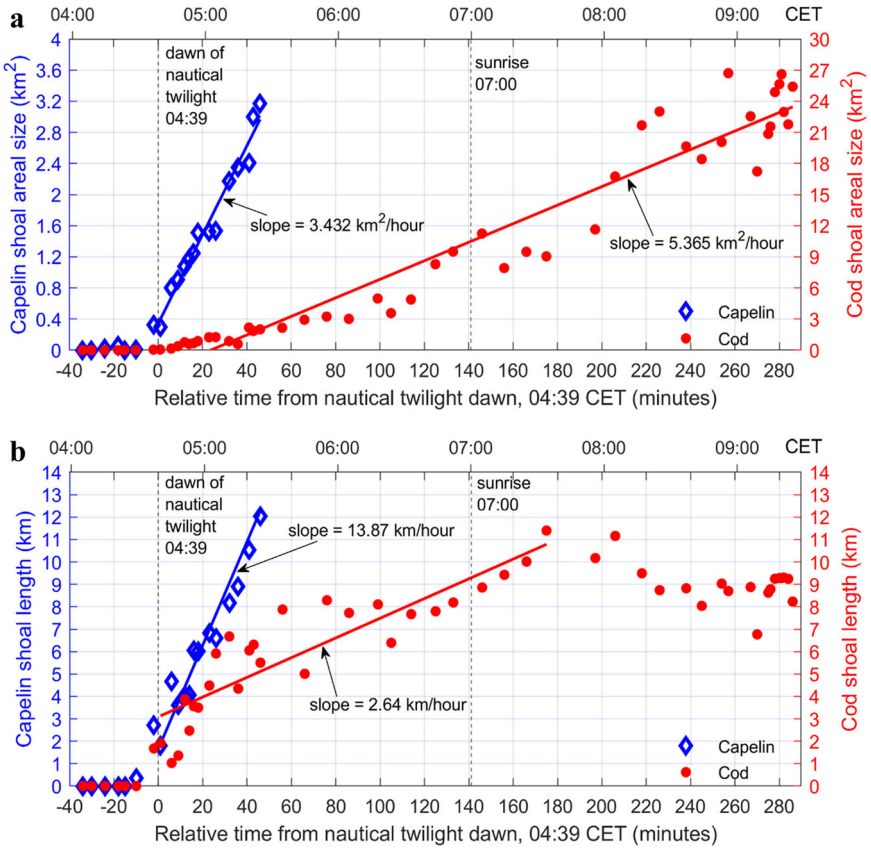

Fig. 4 | Correlated growth in capelin and cod shoals. Area **a** and length **b** of the shoal forming above critical density (1.4 capelin/m^2) for capelin and above critical density (0.06 cod/m^2) for cod. Each shoal propagates with density waves at indicated rates at least an order of magnitude faster than the constituent fish can swim.

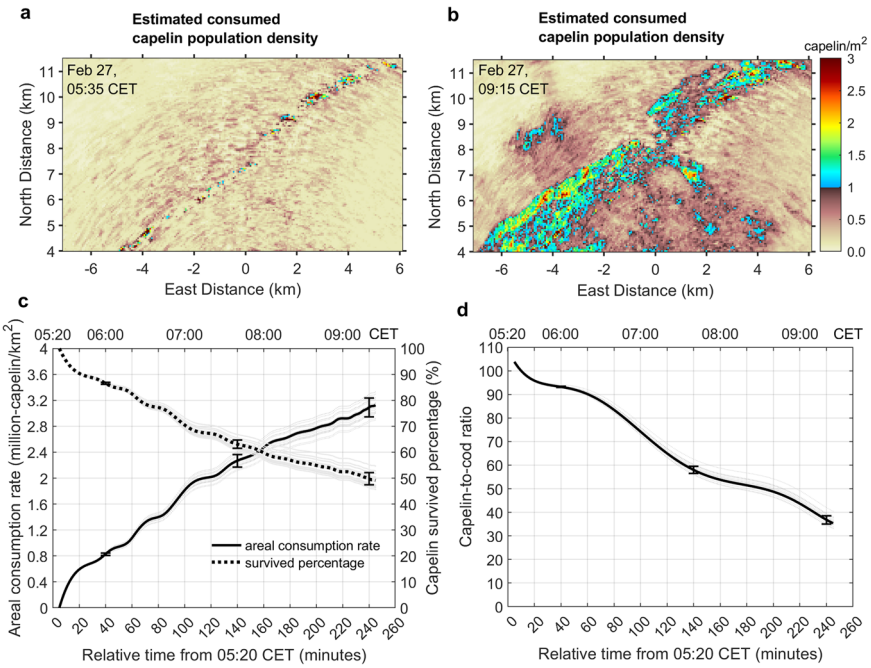

Fig. 5 | Small local behavioural changes rapidly propagate into adversarial shoal engagement that abruptly alters predator-prey balance of tens of millions of keystone Arctic fish within hours. Estimated population density of capelin consumed **a** one hour after dawn twilight during the rapid formation of interacting capelin and cod shoals (Figs. 1–4); and **b** at sunrise (Fig. 1c) when cod shoal population density reaches a peak (Figs. 1–4). Time series of **c** the number of capelin consumed per unit area, percent capelin survived in capelin shoal, and **d** capelin-to-cod population ratio. Predator-prey balance is drastically altered in capelin shoal.

Statistical variation in cod length may result in a possible offset in cod population estimates of ±18% (Methods). Within approximately 4 hours of the capelin attaining critical population density, cod are estimated to consume roughly 10.6 million shoaling capelin with an areal consumption rate of 3.32 million-capelin/km^2. This amounts to a total consumption by cod of approximately 0.1-0.2% of the Barents Sea capelin stock[27] in 4 hours in the capelin shoal.

Our consumption estimates show capelin in the highest density regions have the highest survival rates (Fig. 5a–c). At an enormous scale, this is consistent with observations at much smaller scales that prey within dense groups tend to be at less risk than those in diffuse groups[35–37]. Packing in shoaling fish inhibits predation by visual feeders at daylight[38]. It is possible that such defensive response to cod predation caused formation of the capelin shoal which in turn attracted more cod predators, and the two

correlated processes propagated widely as critical density waves from local inceptions. Such a dynamic process will filter individual capelin that are unable to join the shoal in time, and so enhance survival of the best fit shoaling capelin. The cod in turn thrive through harvesting of capelin less able to complete an energy demanding spawning, and so support a robust ecosystem.

It is also possible that the capelin shoals formed for other reasons such as more efficient migration or group spawning processes, which then also attracted more cod predators and set off the chain reaction of the cod shoal growing in tandem with the capelin shoal. Such group behaviour during spawning highly increases mate-encounter rate which leads to improved mate choice and increased egg fertilization rates as well as time-space alignment to enable synchronized spawning, as has been pointed out for other fish species[11]. When near the bottom, capelin groups possibly also search for seafloor substrates appropriate for spawning. It has been suggested that lineation of migrating groups improves sensing of environmental cues[39].

Discussion

Migrating oceanic fish constitute the world's most productive harvested stocks. They exhibit swarming behaviour, survive via a fine-tuned predator-prey balance where decisive interactions often occur at hotspots of limited spatial extent[3–5]. While the importance of predator-prey interaction is typically known from stomach content studies, the actual behavioural interaction dynamics during predation is not fully understood.

Northeast Arctic cod and capelin are prime examples of abundant, long-migrating, swarming oceanic fish stocks. Our results describe and quantify key processes governing interactions between these species. The group behavioural processes within and across these species and the balance shift at a predation hotspot that follows appear to be essential in the function of this Arctic marine environment. They may also be important for other large ecosystems given the generality of underlying instability mechanisms[6,11]. We show that such processes may dramatically impact the abundance of the prey population, as has been demonstrated in other areas with different methods[4]. Sudden balance shifts may have the potential to affect the stability of an ecosystem already facing anthropogenic and global warming stresses. Climate change, recruitment predation[40] and fisheries management failures[41–43] in the past have triggered the collapse in capelin stock in the Barents Sea, including also the immense capelin and northern cod populations of Canada's Grand Banks, once unparalleled in size and importance but still not recovered after 30 years, as well as other similar collapses[44,45]. Lack of capelin may have catastrophic effect on many higher trophic predators, including marine mammals, larger fish, and sea birds, as has been described in the past[40]. Cod predation prevents excessive food competition among capelin that could compromise their spawning ability given the large distances and high energy reserves required to migrate from their distant ice-edge feeding grounds to coastal Barents Sea spawning grounds, in accord with arms race[46] and selfish herd[32] concepts. Synoptic sensing method such as that employed here can provide new data with sufficiently high spatial and temporal sampling to resolve essential ecosystem processes and aid ocean ecosystem monitoring and modelling. Over time, when proper validation has been completed, we expect this information will be included in resource assessment and management.

Development and implementation of synoptic sensing techniques with sufficient resolution to monitor cross-species interaction enables better assessment of the mechanisms governing group behavioural processes at multiple scales[21]. Predator-prey interaction between capelin and cod[40] with spatial inhomogeneity and temporal variability resulting from dynamic behavioural processes typically associated with predatory hotspots would likely have been missed by conventional survey methods, leading to fundamental knowledge gaps about the presence, causes and propagation of unstable phenomena in this and other important marine environments[3,4]. While the Barents Sea has among the most extensive conventional line-transect surveys of oceanic fish in the world[47], their temporo-spatial sampling is many orders of magnitude below that necessary to independently resolve the wide-area ordered group behavioural mechanisms governing the unstable equilibria and rapid shift in predator-prey balance found here. This is because the synoptic sensing method used here samples at an areal rate many orders of magnitude larger than conventional acoustic line transect methods[7,48].

The fine-tuned competitive relationship between cod and capelin in the Barents Sea, evident in our data, has enabled them both to thrive under challenging environmental conditions in a habitat that supports few species. It involves unstable equilibria in the transition from random to ordered group behaviour between the two species that yield major shifts in predator-prey balance (Fig. 5). Warming from climate change pushes the biologically productive polar front further to the north[49] so extending the distance between coastal spawning and ice-edge feeding areas for both cod and capelin. Both species must adapt to these changes to maintain the ecosystem's stability. Determining the mechanisms governing marine hotspots, formed by the convergence of interacting populations of different species, as observed here, are prerequisite to establishing management priorities[50]. We show that this is achievable by large-scale high-resolution quantitative observation and monitoring of interactions between key species in an Arctic marine hotspot.

While our results are based on a relatively small set of observations, they nevertheless reveal previously unobserved predator-prey interactions over wide areas, and clearly demonstrate the limitations of conventional monitoring strategies to observe and quantify such basic ecosystem processes. Broadband acoustic technologies at much higher frequencies that are well above swimbladder resonance, and exceed 90,000 Hz where attenuation in seawater imposes significant sensing range limitation, have demonstrated capability in studying species interactions but at many orders of magnitude smaller scale than the OAWRS system[51]. We have shown that the formation of vast, dense and spatially discrete behavioural groups of interacting predator and prey occurs by spatially and temporally coincident propagation of critical population density across species. The large-scale group formation observed by OARWS is triggered by changing light conditions when prey become more susceptible to visual predators. The formation of spatially discrete prey behavioural groups when under attack by swarming predators, as observed here over large scales, is advantageous following group behavioural principles well-established at much smaller scales in fish[35]. Species interaction studies for various areas and time periods using OAWRS could facilitate a new and better understanding of the function of large marine ecosystems as well as supporting quantification of key processes in the assessment and management of marine resources over wide areas. The dynamics between species at ecological hotspots are crucial for the function of marine ecosystems[3,4]. If interaction dynamics within hotspots are as important as recent work suggests[3–5,52,53], the approach presented here is well-suited to resolve and quantify such cross-species behavioural processes.

Methods

Scattering strength from measured ocean-acoustic-waveguide remote sensing images

The findings were made possible by imaging of environmental scattering strength that were instantaneously made with ocean-acoustic-waveguide remote sensing over a 75-km diameter region and updated every 50 seconds in a multi-spectral adaptation of Ocean Acoustic Waveguide Remote Sensing (OAWRS). The OAWRS system consisted of a vertical source array and a horizontal receiver array in monostatic arrangement towed by the research vessel Knorr near Finnmark, Norway during February-March 2014 (Fig. 2b). Active source transmissions from the vertical array consisting of eight connected acoustic elements, deployed at depths 60–70 m below sea-surface, are scattered by inhomogeneities in the medium and are received by the horizontal receiver array, towed at depths between 60 and 70 m. The receiver array is made up of three sub-arrays: low frequency aperture, mid frequency aperture and high frequency aperture, each consisting of 64 equally spaced hydrophones with respective hydrophone spacing of 1.5 m,

0.75 m and 0.375 m. Wide-area instantaneous OAWRS images were then generated by beamforming, matched filtering and charting scattered returns. These were used to quantify the population of cod and capelin at each spatial and temporal pixel by use of the distinct resonance frequency characteristics of each species. Instantaneous wide-area scattering strength images zoomed to the region of Supplementary Fig. 1a, for example, were used to determine the population densities of Fig. 1a, b. Frequency responses of each species (Supplementary Fig. 1b) were determined by established theory[8,9,54] given measured fish lengths, swim bladder volumes, and depths from simultaneous capture trawl and echo-sounder measurements which were also used to confirm species and calibrate population densities[6–11]. Linear frequency modulated waveforms of 50 Hz band and 1 second duration were transmitted at six centre frequencies in the roughly octave range between 850 to 1600 Hz spanning the entire resonance peak of the capelin and the upper tail of the cod resonance peak (Supplementary Fig. 1b) to obtain scattered returns from the environment. Scattering strength at each pixel was determined from these using parabolic equation propagation modelling with measured bathymetry and oceanography[7,55].

Calculation of scattering strength $SS(\boldsymbol{\rho}, f_j)$ at horizontal location $\boldsymbol{\rho}$ and frequency f_j is shown in Supplementary Information section 1. Scatter functions of capelin and cod were obtained from standard theory[54] with local in-situ measurements of shoal occupancy depths from RV Knorr echosounder and measured fish length distributions. Cod length distribution is obtained from the Institute of Marine Research (IMR) January-March 2014 winter survey report[34] from the acoustic and trawl catch abundance measurements in the area between 70° to 72° N and 17° to 31° E which roughly encompasses the region surveyed by OAWRS in the Barents Sea and includes the zoomed area shown in Fig. 1a, b. The mean length of cod in the area was calculated from the survey report[34] in the following way: The age distribution of cod, acoustic and bottom trawl estimates combined from merged survey areas B and C[34] which contain the location of the experiment, was combined with the mean length at age in those areas to obtain mean cod length of approximately 61 cm with a standard deviation of 13 cm. Conventional acoustic abundance estimates of mature spawning capelin categorized by length in the ICES Arctic Fisheries Working Group 2014 report[27] were used to obtain capelin length distribution whose mean and standard deviation were found to be 15.4 cm and 1 cm respectively. Capelin individuals with lengths 14 cm or greater are considered mature[27]. Neutral buoyancy depths, 7 m for capelin and 280 m for cod, were determined by maximum likelihood estimation using respective measured scattering strength data and the known physical model of resonant scattering for each species. Resonant acoustic scattering from swimbladder-bearing fish at wavelengths large compared to the swimbladder requires simple damped harmonic oscillator modelling. Only a small number of physical parameters such as swimbladder shape, fish flesh density, viscosity and ambient pressure are needed to accurately model such low frequency resonant scattering[9,54,56]. Multiple at-sea experiments with hundreds to thousands of independent data points have demonstrated the validity of this resonant scattering model in correlating acoustic measurements and fish biological data[9–11,56–58]. The model is also in good agreement with data collected in the Barents Sea during the experiment of the current analysis, for scattering strength measurements across six distinct frequencies (Supplementary Fig. 1).

Capelin and cod areal population density estimation

Capelin and cod population densities at each pixel were determined by maximum likelihood estimation given the multi-spectral scattering strength data and the known physical model of resonant scattering for each species and its measured parameters. Individual cod are spaced widely enough to be seen under small near-surface capelin groups before and at dawn in the conventional echograms (Fig. 1c), where the cod are roughly 10–30 m apart horizontally and the small capelin groups are 50–100 m in length with similar spacings. The underwater remote sensing imagery (Fig. 1a, b) then roughly resolves individual predator interactions with prey since its resolution is roughly 15 m in range and 0.3° in horizontal azimuth[56,59], which translates to roughly 30–60 m cross-range resolution at 5–10 km from the sensor, as is often the case for the shoals studied here. We employed array aperture windowing to reduce beamforming sidelobes, leading to roughly 0.5° in azimuthal resolution, or 40–80 m cross-range resolution at 5–10 km, maintaining 15 m range resolution, still at roughly the scale of individual cod spacings just before capelin shoal formation at dawn.

Areal population densities of capelin and cod at each pixel were inferred from the measured scattering strength at that pixel using the maximum likelihood estimation method. For any pixel at horizontal location $\boldsymbol{\rho}$, two parameters are to be estimated: areal population density of capelin $n_{A_{capelin}}$ and areal population density of cod $n_{A_{cod}}$. Here, scattering strength measurements at any pixel are found to be Gaussian random variables as converged upon by the central limit theorem such that standard deviation is independent of the mean, consistent with variance stabilization by log transformation of normalized field intensity data[6–8,60]. Then, the multivariate Gaussian log-likelihood function[61] for an N_f-dimensional vector of scattering strength measurements $SS = [SS(\boldsymbol{\rho}, f_1), SS(\boldsymbol{\rho}, f_2), \ldots, SS(\boldsymbol{\rho}, f_{Nf})]$ for frequencies $f_1, f_2, \ldots, f_{N_f}$ at any pixel can be expressed as

$$l\left(n_{A_{capelin}}, n_{A_{cod}}\right) = \sum_{j=1}^{N_f} \left\{ -\frac{1}{2} \frac{\left(SS\left(\boldsymbol{\rho}, f_j\right) - <SS\left(\boldsymbol{\rho}, f_j | n_{A_{capelin}}, n_{A_{cod}}\right)>\right)^2}{\sigma_{f_j}^2} - \frac{1}{2}\log\left(2\pi\sigma_{f_j}^2\right) \right\} \tag{1}$$

Here, $\langle SS(\boldsymbol{\rho}, f_j | n_{A_{capelin}}, n_{A_{cod}})\rangle$ is the expected scattering strength (see Supplementary Information section 1) and $\sigma_{f_j}^2$ is the variance of measured scattering strength at frequency $f_j, j = 1, 2, \ldots, N_f = 6$. Mean measured scattering strength from representative regions dominated by capelin, cod and capelin-cod mixture as marked in Supplementary Fig. 1a are plotted as a function of frequency in Supplementary Fig. 1b, each matching theoretically expected resonance spectra with correlation coefficients of 0.98, 0.93 and 0.95 respectively. Measured scattering strength frequency response of capelin-cod mixture in Supplementary Fig. 1b is obtained from scattering strength data at 05:35 CET within the corresponding region marked in Supplementary Fig. 1a.

Optimal estimates $\hat{n}_{A_{cp}}$ and $\hat{n}_{A_{cd}}$ of the areal population densities $n_{A_{capelin}}$ and $n_{A_{cod}}$ were determined by an exhaustive search over the ranges of capelin and cod population densities such that the log-likelihood function in Eq. (1) was maximized. This is equivalent to minimizing the magnitude of the weighted sum of square difference between the measured scattering strength and expected scattering strength:

$$\min_{n_{A_{capelin}}, n_{A_{cod}}} \left| \sum_{j=1}^{N_f} \left\{ -\frac{1}{2} \frac{\left(SS\left(\boldsymbol{\rho}, f_j\right) - \left\langle SS\left(\boldsymbol{\rho}, f_j | n_{A_{capelin}}, n_{A_{cod}}\right)\right\rangle\right)^2}{\sigma_{f_j}^2} \right\} \right| \tag{2}$$

Areal population densities of capelin and cod thus obtained were mapped over all pixels and presented in Fig. 1. Population density estimates for each species were found to have per-pixel error from Gaussian field fluctuations of roughly 1 dB[6–8,11,62] and a systematic root mean-square offset error on all pixels through capelin and cod size variations (Methods section 1) of roughly 25–40 percent. The root-mean-square errors are estimated by averaging 100 Monte-Carlo simulations of scatter functions of capelin and cod where each simulation employs a realization of occupancy depth for an individual fish from a uniformly distributed vertical shoal layer and a realization of fish length from its distribution. Co-registration of capelin shoals in OAWRS population density images and independent echosounder measurements from research vessel RV Johan Hjort is shown in Supplementary Fig. 2. Exact correspondence and match between population density estimates from OAWRS and

conventional surveys have been repeatedly shown previously for large aggregations of fish species such as Northeast Arctic cod, Norwegian spring-spawning herring, Atlantic herring with hundreds to thousands of independent OAWRS samples and tens of thousands of independent conventional fisheries echosounder samples[6,7,9,11].

Estimated cod predation on capelin

We estimate the number of capelin consumed by cod as well as those survived as a function of space and time (Fig. 5a, b) using instantaneous wide-area population density measurements for each species over time. Before dawn twilight, capelin in surface layers and cod below are assumed to have negligible interaction based on echogram data and the context that cod are visual predators. In our estimates, cod feeding effectively begins when capelin descend to the depths inhabited by cod, at mean capelin layer depth roughly 50 m below the sea surface an hour after dawn at 5:30 CET when lighting enables visual predation. Cod average depths were stable in the lower part of the water column for remote sensing throughout all periods investigated. Within any temporo-spatial resolution cell the consumed capelin and survived capelin populations are estimated. Consumption is taken to be only a function of surviving capelin and cod entering a temporo-spatial cell when the two species are in the same depth layers. Each newly entering cod is expected to consume up to 9 capelin as available in that cell, based on our in-situ cod samples and other similar measurements[14]. The gas-filled swimbladders of capelin, with only air in-take from the sea surface, compress via Boyles law as they descend. At times beyond 5:35 CET capelin target strengths become too small for capelin population density to be updated by the remote sensing system due their continued descent. After this time, capelin kinematics and survived population density are estimated. The estimates are based on the last remotely measured capelin population densities at 5:35 CET, and their subsequent consumption by cod. Cod population density was robustly measured by ocean-acoustic waveguide remote sensing at all times.

We obtain quantitative estimates of cod predation on capelin using OAWRS population density images of both capelin and cod with a predation model which assumes cod that have converged on locations of capelin arrive there to prey on the capelin. Echogram measurements show cod occupy vertical depths from 50 m below sea-surface down to the seafloor. In our predation estimates, capelin consumption occurs when capelin enter cod depth layers after undertaking downward migration from the sea-surface at 05:25 CET. Within a resolution cell of area A m^2 with capelin population density $n_{A_{capelin}}$ $fish/m^2$ and cod population density $n_{A_{cod}}$ $fish/m^2$, the estimated consumed capelin population density at any time instant t_{n+1}, $n^{consumed}_{A_{capelin}}(t_{n+1})$, is only a function of surviving capelin and new cod entering a spatial cell between times t_n and t_{n+1}. So when the two species are in the same depth layers i.e. depths greater than 50 m, $n^{consumed}_{A_{capelin}}(t_{n+1}) = \gamma[n_{A_{cod}}(t_{n+1}) - n_{A_{cod}}(t_n)]$ when $n_{A_{cod}}(t_{n+1}) > n_{A_{cod}}(t_n)$, otherwise $n^{consumed}_{A_{capelin}}(t_{n+1}) = 0$, such that $n^{consumed}_{A_{capelin}}(t_{n+1}) \le n^{survived}_{A_{capelin}}(t_n)$ for $n \ge 0$. The predation model assumes that all new cod entering the resolution cell prey on the available capelin. This is because we cannot track individual fully fed cod that may enter from another resolution cell. The estimated survived capelin population density at time t_{n+1}, $n^{survived}_{A_{capelin}}(t_{n+1}) = n^{survived}_{A_{capelin}}(t_n) - n^{consumed}_{A_{capelin}}(t_{n+1})$ and the cumulative consumed capelin population density at time t_{n+1}, $n^{consumed,total}_{A_{capelin}}(t_{n+1}) = \sum_{k=1}^{n+1} n^{consumed}_{A_{capelin}}(t_k)$ are then computed at every spatial cell and plotted in Fig. 5a, b. Capelin and cod population densities at 05:35 CET are taken to be inputs $n_{A_{capelin}}(t_0)$ and $n_{A_{cod}}(t_0)$ respectively at time t_0 such that $n^{consumed}_{A_{capelin}}(t_0) = \gamma n_{A_{cod}}(t_0)$ when $\gamma n_{A_{cod}}(t_0) \le n_{A_{capelin}}(t_0)$, otherwise $n^{consumed}_{A_{capelin}}(t_0) = n_{A_{capelin}}(t_0)$. Then the number of survived capelin at t_0 is $n^{survived}_{A_{capelin}}(t_0) = n_{A_{capelin}}(t_0) - n^{consumed}_{A_{capelin}}(t_0)$. The following estimates of survived capelin population densities at times t_{n+1} when $n \ge 0$ are based on the last capelin population densities measured by OAWRS at 5:35 CET, and their subsequent consumption by cod. Observations from RV Knorr echograms (Fig. 2c) show an increase in capelin packing densities during their descent towards the seafloor. Estimation error bars in Fig. 5c, d account for the uncertainty in capelin population density. The upper part of the error bar is computed by assuming capelin densities above 0.4 capelin/m^2 have uniformly increased by 1 capelin/m^2 from the last measurement at 05:35 CET such that the total capelin population within the rectangular region of Fig. 1 remains unchanged. The lower part of the error bar assumes no change in capelin densities from last measurement at 05:35 CET.

Historical cod stomach sample records from the Barents Sea[14,63] were used to determine the mean capelin weight consumed by an individual cod. These cod stomach content records were obtained from areas where cod and capelin overlapped spatially. Measurements of capelin weight in these cod stomachs as a function of cod length provided information for the consumption analysis and estimates of this paper. From the dataset provided in Ref. 63, we examined stomach sample records of cod individuals between the length range 48–74 cm i.e., up to one standard deviation of 13 cm above and below mean cod length of 61 cm[34]. We further restricted our analysis to cod sample records with only capelin prey in their stomachs. The mean capelin weight consumed by an individual cod is then found to be approximately 155 g. This corresponds to the weight of roughly 9 spawning capelin individuals where the average weight of an individual spawning capelin is 18 g and its mean length is 15.4 cm[27]. Subsequently, a value of $\gamma = 9$ is used in our predation estimates. See Supplementary Information for further details. This is compatible with findings in Magnusson and Aspelund[64] where a similar number of approximately 8 capelin consumed by an individual mid-sized cod between lengths 61–70 cm is obtained when the average number of capelin captured by cod in an encounter with a capelin school is multiplied with the average number of encounters with capelin schools over the time taken to completely digest capelin.

This study was approved by the animal ethics committee of the Institute of Marine Research (IMR) and granted permission by the Government of Norway's National Joint Headquarters on January 28 2014 and conducted with the IMR's and Norway's ethical guidelines for such studies. We have complied with all relevant ethical regulations for animal use.

Statistics and reproducibility

Exact correspondence and match between population density estimates from OAWRS and conventional surveys have been repeatedly shown for large fish shoals in regions including the Nordic Seas, Gulf of Maine, and Mid-Atlantic Bight[6,7,9,11,58]. Each instantaneous OAWRS image consists of hundreds of thousands of independent pixels with 15 m range resolution from matched filter and with 64 independent horizontal beams, spanning roughly 50 km in range. The angular resolution varies as $\lambda/(L\cos\theta)$ away from endfire, where λ is the acoustic wavelength, L is the receiver array aperture length and θ is the horizontal angle from array broadside which is normal to the receiver array axis[7–9]. Then in each of the instances where massive aggregations of fish species such as Northeast Arctic cod, Norwegian spring-spawning herring, Atlantic herring were found[6,7,9,11,58], co-registration of fish groups in the OAWRS and conventional fish-finding sonar (CFFS) systems was shown with hundreds to thousands of independent OAWRS samples and tens of thousands of independent CFFS samples.

Expected two-way transmission loss over fish shoal depths in various continental shelf environments with measured bathymetry and oceanography have been shown to be relatively stable and accurately understood[6,8,9,65]. The parabolic equation model used to estimate wide-area transmission loss for an ocean-acoustic waveguide has been calibrated with thousands of transmission loss measurements over varying ranges from 100 s of m to 10 s of kms[9,65]. Then the OAWRS population density estimates for each species were found to have a root mean-square error offset on all pixels of roughly 25–40 percent by averaging 100 Monte-Carlo simulations of capelin and cod scatter functions. Each simulation employs a realization of occupancy depth for an individual fish from a uniformly distributed

vertical shoal layer and a realization of fish length following the distributions of capelin and cod sizes. Only the length of each fish was changed randomly in each simulation realization.

Capelin population density estimates made by multispectral OAWRS in Figs. 1–5 are found to have a potential offset of roughly ±25% based on measured variations in capelin length and volume. The percentage error offset is estimated in capelin population density obtained from multispectral OAWRS data due to measured variances in capelin length and volume in the Barents sea experimental location and season[27]. Population density estimates are based on OAWRS frequency measurements of 50 Hz bandwidth at six centre frequencies which are at or near swimbladder resonance (Figure S1, and Methods). At these frequencies the acoustic wavelength is much larger than the swimbladder, capelin scattering amplitude is proportional to swimbladder volume[54,66], which in turn has a well-known relationship to fish length and fish volume for physostome fish[67–70] including capelin[71]. The percentage error is determined with respect to the experimentally measured value of population density we obtained based on comparison between OAWRS and conventional fisheries echosounder data in Figure S2.

Similarly, cod population density estimates made by multispectral OAWRS in Figs. 1–5 are found to have a potential offset of roughly ±18% based on measured variations in cod length and volume in the Barents sea experimental location and season[34]. The percentage error is determined with respect to the experimentally measured value of population density we obtained based on the OAWRS and conventional echosounder data shown in Supplementary Fig. 2. Additionally, the error in our cod population density estimates due to contamination from haddock is found to be less than 10%. The percentage error is determined based on OAWRS scattering analysis with mixed species[9] using measured haddock length distribution in the Barents Sea experimental location and time period[34] using an upper bound of 20% haddock mixed with the cod populations. Contamination from herring, blue whiting and Sebastes, as observed by the simultaneous winter survey[34], is found to be negligible making total contamination from other species than cod less than 10%.

Reporting summary

Further information on research design is available in the Nature Portfolio Reporting Summary linked to this article.

Data availability

All data are available in the main text, Methods, Supplementary Information or Supplementary Data. Numerical source data for figures in the manuscript can be found in Supplementary Data 1-4.

Code availability

Codes are available at https://doi.org/10.5281/zenodo.13298961[72].

Received: 9 December 2023; Accepted: 24 September 2024;
Published online: 29 October 2024

References

1. Nakken, O. Norwegian spring-spawning herring & northeast arctic cod: 100 years of research and management. Tapir Academic Press, Trondheim. 177 s., ill. (2008).
2. Gjøsæter, H. The population biology and exploitation of capelin (*Mallotus villosus*) in the Barents Sea,. *Sarsia* **83**, 453–496 (1998).
3. Davoren, G. K. Distribution of marine predator hotspots explained by persistent areas of prey. *Mar. Biol.* **160**, 3043–3058 (2013).
4. Temming, A., Floeter, J. & Ehrich, S. Predation hot spots: large scale impact of local aggregations. *Ecosystems* **10**, 865–876 (2007).
5. Worm, B., Lotze, H. K. & Myers, R. A. Predator diversity hotspots in the blue ocean. *Proc. Natl Acad. Sci. USA* **100**, 9884–9888 (2003).
6. Makris, N. C. et al. Critical population density triggers rapid formation of vast oceanic fish shoals. *Science* **323**, 1734–1737 (2009).
7. Makris, N. C. et al. Fish population and behaviour revealed by instantaneous continental shelf-scale imaging. *Science* **311**, 660–663 (2006).
8. Jagannathan, S. et al. Ocean acoustic waveguide remote sensing (OAWRS) of marine ecosystems. *Mar. Ecol. Prog. Ser.* **395**, 137–160 (2009).
9. Gong, Z. et al. Low-frequency target strength and abundance of shoaling Atlantic herring (Clupea harengus) in the Gulf of Maine during the Ocean Acoustic Waveguide Remote Sensing 2006 Experiment. *J. Acoustical Soc. Am.* **127**, 104–123 (2010).
10. Wang, D. et al. Vast assembly of vocal marine mammals from diverse species on fish spawning ground. *Nature* **531**, 366–370 (2016).
11. Makris, N. C. et al. Instantaneous areal population density of entire Atlantic cod and herring spawning groups and group size distribution relative to total spawning population. *Fish. Fish.* **20.2**, 201–213 (2019).
12. Bogstad, B. & Gjøsæter, H. Predation by cod (Gadus morhua) on capelin (Mallotus villosus) in the Barents Sea: implications for capelin stock assessment. *Fish. Res.* **53**, 197–209 (2001).
13. Maunder, M. N. & Piner, K. R. Contemporary fisheries stock assessment: many issues still remain. *ICES J. Mar. Sci.* **72**, 7–18 (2015).
14. Fall, J., Johannesen, E., Englund, G., Johansen, G. O. & Fiksen, Ø. Predator–prey overlap in three dimensions: cod benefit from capelin coming near the seafloor. *Ecography* **44**, 802–815 (2021).
15. Vicsek, T., Czirók, A., Ben-Jacob, E., Cohen, I. & Shochet, O. Novel type of phase transition in a system of self-driven particles. *Phys. Rev. Lett.* **75**, 1226–1229 (1995).
16. Couzin, I., Krause, J., Franks, N. R. & Levin, S. A. Effective leadership and decision-making in animal groups on the move. *Nature* **433**, 513–516 (2005).
17. Buhl, J. et al. From disorder to order in marching locusts. *Science* **312**, 1402–1406 (2006).
18. Ostermann, M. et al. Early Holocene (8.6 ka) rock avalanche deposits, Obernberg valley (Eastern Alps): Landform interpretation and kinematics of rapid mass movement. *Geomorphology* **171-172**, 83–93 (2012).
19. Geller, R. J., Jackson, D. D., Kagan, Y. Y. & Mulargia, F. Earthquakes Cannot Be Predicted. *Science* **275**, 1616 (1997).
20. Pyle, D. M. Mass and energy budgets of explosive volcanic eruptions. *Geophys. Res. Lett.* **22**, 563–566 (1995).
21. Godø, O. R. et al. Marine ecosystem acoustics (MEA): quantifying processes in the sea at the spatio-temporal scales on which they occur. *ICES J. Mar. Sci.* **71**, 2357–2369 (2014).
22. Savoca, M. S. et al. Baleen whale prey consumption based on high-resolution foraging measurements. *Nature* **599**, 85–90 (2021).
23. Hunsicker, M. E. et al. Functional responses and scaling in predator-prey interactions of marine fishes: contemporary issues and emerging concepts. *Ecol. Lett.* **14**, 1288–1299 (2011).
24. Reed, S. E. et al. Foliar nematode, *Litylenchus crenatae* ssp. *mccannii*, population dynamics in leaves and buds of beech leaf disease-affected trees in Canada and the US. *Path.* **50**, e12599 (2020).
25. Hastings, A. et al. Transient phenomena in ecology. *Science* **361**, eaat6412 (2018).
26. Marras, S. et al. Fish swimming in schools save energy regardless of their spatial position. *Behavioural Ecol. Sociobiol.* **69**, 19–226 (2015).
27. ICES. Report of the Arctic Fisheries Working Group (AFWG). https://doi.org/10.17895/ices.pub.19282478 (2014).
28. Serebrov, L. I. On density of distribution and orientation of capelin in schools. in *Proc Soviet-Norwegian Symp on the Barents Sea Capelin*, Gjosaeter, H., Ed. (Institute of Marine Research, Bergen 1985), pp 157–170 (1984).

29. Misund, O. A. Dynamics of moving masses: variability in packing density, shape, and size among herring, sprat, and saithe schools. *ICES J. Mar. Sci.* **50**, 145–160 (1993).
30. Pitcher, T. & Partridge, B. Fish school density and volume. *Mar. Biol.* **54**, 383–394 (1979).
31. Major, P. F. Predator-prey interactions in two schooling fishes, Caranx ignobilis and Stolephorus purpureus. *Anim. Behav.* **26**, 760–777, https://linkinghub.elsevier.com/retrieve/pii/0003347278901422 (1978).
32. King, A. J. et al. Selfish-herd behaviour of sheep under threat. *Curr. Biol.* **22**, R561–R562 (2012).
33. Hawkins, A. D. & Picciulin, M. The importance of underwater sounds to gadoid fishes. *J. Acoustical Soc. Am.* **146**, 3536–3551 (2019).
34. Mehl, S. et al. Fish investigations in the Barents Sea winter 2013-2014. *IMR/PINRO Jt. Rep. Ser.* **2014**, 73 (2014).
35. Pitcher, T. J. "Functions of Shoaling Behaviour in Teleosts" in *The Behaviour of Teleost Fishes*, T. J. Pitcher, Ed. (Springer US, 1986), pp. 294–337.
36. Ioannou, C. C., Guttal, V. & Couzin, I. D. Predatory fish select for coordinated collective motion in virtual prey. *Science* **337**, 1212–1215 (2012).
37. Handegard, N. O. et al. The dynamics of coordinated group hunting and collective information transfer among schooling prey. *Curr. Biol.* **22**, 1213–1217 (2012).
38. Rieucau, G., Holmin, A. J., Castillo, J. C., Couzin, I. D. & Handegard, N. O. School level structural and dynamic adjustments to risk promote information transfer and collective evasion in herring. *Anim. Behav.* **117**, 69–78 (2016).
39. Berdahl, A., Torney, C. J., Ioannou, C. C., Faria, J. J. & Couzin, I. D. Emergent sensing of complex environments by mobile animal groups. *Science* **339**, 574–576 (2013).
40. Gjøsæter, H., Hallfredsson, E. H., Mikkelsen, N., Bogstad, B. & Pedersen, T. Predation on early life stages is decisive for year-class strength in the Barents Sea capelin (Mallotus villosus) stock. *ICES J. Mar. Sci.* https://doi.org/10.1093/icesjms/fsv177 (2015).
41. Rose, G. A. *Cod: the ecological history of the North Atlantic fishery* (Breakwater Books, 2007).
42. Rose, G. A. Fisheries Resources and Science in Newfoundland and Labrador: An Independent Assessment. *Royal Commission on Renewing and Strengthening Our Place in Canada* (2003).
43. Mullowney, D. R. J., Dawe, E. G., Colbourne, E. B. & Rose, G. A. A review of factors contributing to the decline of Newfoundland and Labrador snow crab (*Chionoecetes opilio*). *Rev. Fish. Biol. Fish.* **24**, 639–657 (2014).
44. Pershing, A. J. et al. Slow adaptation in the face of rapid warming leads to collapse of the Gulf of Maine cod fishery. *Science* **350**, 809–812 (2015).
45. Richards, R. A. & Hunter, M. Northern shrimp *Pandalus borealis* population collapse linked to climate-driven shifts in predator distribution. *PLoS ONE* **16**, e0253914 (2021).
46. Guo, L. et al. Convergent resistance to GABA receptor neurotoxins through plant–insect coevolution. *Nat. Ecol. Evol.* **7**, 1444–1456 (2023).
47. Eriksen, E. et al. From single species surveys towards monitoring of the Barents Sea ecosystem. *Prog. Oceanogr.* **166**, 4–14 (2018).
48. Makris, N. C. et al. Fish population and behaviour revealed by instantaneous continental shelf-scale imaging. *Science* **311**, 660–663 (2006). Supplementary Material.
49. Ingvaldsen, R. B. et al. Physical manifestations and ecological implications of Arctic Atlantification. *Nat. Rev. Earth Environ.* **2**, 874–889 (2021).
50. Hazen, E. L. et al. Scales and mechanisms of marine hotspot formation. *Mar. Ecol. Prog. Ser.* **487**, 177–183 (2013).
51. Skaret, G. et al. Diel vertical movements determine spatial interactions between cod, pelagic fish and krill on an Arctic shelf bank. *Mar. Ecol. Prog. Ser.* **638**, 13–23 (2020).
52. Krause, J. et al. Injury-mediated decrease in locomotor performance increases predation risk in schooling fish. *Philos. Trans. R. Soc. B: Biol. Sci.* **372**, 20160232 (2017).
53. Ramírez, F., Afán, I., Davis, L. S. & Chiaradia, A. Climate impacts on global hot spots of marine biodiversity. *Sci. Adv.* **3**, 1–7 (2017).
54. Love, R. H. Resonant acoustic scattering by swimbladder-bearing fish. *J. Acoustical Soc. Am.* **64**, 571–580 (1978).
55. Collins, M. D. A split-step Padé solution for the parabolic equation method. *J. Acoustical Soc. Am.* **93**, 1736–1742 (1993).
56. Yi, D. H., Gong, Z., Jech, J. M., Ratilal, P. & Makris, N. C. Instantaneous 3D continental-shelf scale imaging of Oceanic fish by multi-spectral resonance sensing reveals group behaviour during spawning migration. *Remote Sensing*, **10**, (2018).
57. Love, R. "Response to "Comment on 'Resonant acoustic scattering by swimbladder-bearing fish'" [J. Acoust. Soc. Am. 64, 571-580 (1978)]."*. J. Acoustical Soc. Am.* **134**, 3399–3402 (2013).
58. Duane, D., Godø, O. R. & Makris, N. C. Quantification of wide-area Norwegian spring-spawning herring population density with Ocean Acoustic Waveguide Remote Sensing (OAWRS). *Remote Sens* **13**, 4546 (2021).
59. Wang, D., Ratilal, P. Angular resolution enhancement provided by nonuniformly-spaced linear hydrophone arrays in ocean acoustic waveguide remote sensing. *Remote Sensing* **9**, (2017).
60. Pednekar, S., Krishnadas, A., Cho, B. & Makris, N. C. Weber's Law of perception is a consequence of resolving the intensity of natural scintillating light and sound with the least possible error. *Proc. R. Soc. A.* **479**, 20220626 (2023).
61. Rao, C. R. Linear statistical inference and its applications (Wiley New York, 1973).
62. Makris, N. C. The effect of saturated transmission scintillation on ocean acoustic intensity measurements. *J. Acoustical Soc. Am.* **100**, 769–783 (1996).
63. Fall, J., Johannesen, E., Englund, G., Johansen, G. O. & Fiksen Ø. Predator-prey overlap in three dimensions: cod benefit from capelin coming near the seafloor [Dataset]. Dryad https://doi.org/10.5061/dryad.4j0zpc89q (2021).
64. Magnússon, K. G. & Aspelund, T. A model for estimating meal frequency and meal size from stomach data with an application to Atlantic cod (*Gadus morhua*) feeding on capelin (*Mallotus villosus*). *Can. J. Fish. Aquat. Sci.* **54**, 876–889 (1997).
65. Andrews, M., Chen, T. & Ratilal, P. Empirical dependence of acoustic transmission scintillation statistics on bandwidth, frequency, and range in New Jersey continental shelf. *J. Acoust. Soc. Am.* **125**, 111–124 (2009).
66. Rayleigh, J. W. S. *The Theory of Sound Vol II*, (Macmillan UK 1896) Ch 7 Section 335.
67. Nero, R. W., Thompson, C. H. & Jech, J. M. In situ acoustic estimates of the swimbladder volume of Atlantic herring (Clupea harengus). *ICES J. Mar. Sci.* **61**, 323–337 (2004).
68. Ona, E., Zhao, X., Svellingen, I. & Fosseidengen, J. E. Seasonal Variation in Herring Target Strength. *Alaska Sea Grant College Program*, Herring: E: 461–488 (2001).
69. Bertrand, A. & Josse, E. Tuna target-strength related to fish length and swimbladder volume. *ICES J. Mar. Sci.* **57**, 1143–1146 (2000).
70. Schaefer, K. M. & Oliver, C. W. Shape, volume, and resonance frequency of the swimbladder of yellowfin tuna, Thunnus albacares. *Fish. Bull.* **98**, 364–374 (2000).
71. Jørgensen, R. The effects of swimbladder size, condition and gonads on the acoustic target strength of mature capelin. *ICES J. Mar. Sci.* **60**, 1056–1062 (2003).
72. Pednekar, S. S. (2024). Codes for figures in "Rapid predator-prey balance shift follows critical-population-density transmission

between cod (Gadus morhua) and capelin (Mallotus villosus)". (Matlab 2018). Zenodo. https://doi.org/10.5281/zenodo.13298961.
73. Maclennan, D. N., Fernandes, P. G. & Dalen, J. A consistent approach to definitions and symbols in fisheries acoustics. *ICES J. Mar. Sci.* **59**, 365–369 (2002).

Acknowledgements
This work was funded by Office of Naval Research and Institute of Marine Research, Norway.

Author contributions
Analysis and development shared by all authors; at sea exploration, discovery, experimental data collection and preliminary analysis N.C.M., O.R.G and A.J.; S.P. reduced, processed, investigated and displayed experimental data with guidance from N.C.M.; N.C.M, and O.R.G. conceived the experiment; N.C.M., O.R.G. and S.P. wrote the manuscript; S.P. wrote the online methods section with contributions from all authors; N.C.M. and O.R.G. supervised overall project and obtained the funding.

Competing interests
The authors declare no competing interests.

Additional information
Supplementary information The online version contains supplementary material available at https://doi.org/10.1038/s42003-024-06952-6.

Correspondence and requests for materials should be addressed to Nicholas C. Makris.

Peer review information *Communications Biology* thanks Bjarte Bogstad and the other, anonymous, reviewers for their contribution to the peer review of this work. Primary Handling Editors: Eoin O'Gorman, Luke Grinham and Johannes Stortz.